Optical Engineering

OpticalEngineering.SPIEDigitalLibrary.org

Iterative intersymbol interference cancellation in vestigial sideband Nyquist–subcarrier modulation system

Na Liu
Xue Chen
Cheng Ju
Rongqing Hui

SPIE.

Iterative intersymbol interference cancellation in vestigial sideband Nyquist–subcarrier modulation system

Na Liu,[a,*] Xue Chen,[a] Cheng Ju,[a] and Rongqing Hui[b]
[a]Beijing University of Posts and Telecommunications, State Key Lab of Information Photonics and Optical Communications, P.O. Box 128, #10 XiTuCheng Road, HaiDian District, Beijing 100876, China
[b]University of Kansas, Department of Electrical Engineering and Computer Science, 3026 Eaton Hall, 1520 W. 15th Street, Lawrence, Kansas 66045, United States

Abstract. The intersymbol interference caused by dispersion, chirp, and a vestigial sideband filter in intensity modulation and a direct detection single carrier system is analyzed theoretically and numerically. An iterative nonlinear intersymbol interference cancellation technique is proposed and experimentally demonstrated in a 40-Gbps 16-QAM Mach-Zehnder modulator-based vestigial sideband intensity modulation and direct detection half-cycle Nyquist–subcarrier modulation system over a 100-km uncompensated standard single-mode fiber transmission for the first time. The experimental results show that 2.2-dB receiver sensitivity improvement is obtained at the forward error correction limit by using the iterative technique. [DOI: 10.1117/1.OE.53.11.116109]

Keywords: intensity modulation; direct detection; vestigial sideband; intersymbol interference.

Paper 141412 received Sep. 11, 2014; accepted for publication Oct. 17, 2014; published online Nov. 12, 2014.

1 Introduction

The increasing demand to achieve both higher bit rates and spectral efficiency using cost-effective systems is especially strong in short-range communication. Intensity modulation and direct detection (IMDD) based optical communication systems with high-order modulation formats have continued to attract attention because of the low cost and simple implementation, such as a half-cycle Nyquist–subcarrier modulation (SCM).[1,2] For a double sideband (DSB) signal, the dispersion power penalty caused by dispersive transmission with direct detection limits the transmission distance.[3] Without an expensive optical dispersion compensator, optical vestigial sideband (VSB) filtering is a more practical and desirable method for improving the chromatic dispersion tolerance[4,5] and the spectral efficiency of a dense wavelength division multiplexing system.[6] However, the square-law detection of the VSB signal still induces intersymbol interference (ISI), which degrades the transmission performance.

Electrical equalization methods have been widely explored to suppress the ISI generated by chromatic dispersion, such as feed-forward equalizers (FFE), decision feedback equalizers (DFE),[7] and frequency-domain equalization (FDE).[8,9] But they cannot fully compensate the distortions because the absolute square-law detection of the photodiode (PD) is the fundamental reason why the performance of conventional linear equalizer is degraded. A nonlinear equalizer is used to further enhance the system performance, such as a mathematical square root operator (SQRT),[10] nonlinear FFE-DFE (NL-FFE-DFE),[11] and maximum-likelihood sequence estimation (MLSE).[12,13] SQRT can linearize the receiver before equalization, but this cannot change the fact that the phase information introduced by dispersion is lost even after the square root operation. NL-FFE-DFE can be considered to be an extension from the normal DFE with both an FFE filter and a DFE filter. Compared with SQRT and NL-FFE-DFE, a better performance can be obtained by using an MLSE with a higher complexity.

In this paper, a theoretical model[14] is first established to investigate the dispersion-, chirp, VSB filter-induced ISI in a VSB-IMDD single carrier system. In more detail, the ISI can be divided into two parts, namely the linear part and the nonlinear part. A conventional electrical dispersion compensation method, overlap FDE (O-FDE),[8] is used to compensate the linear distortion. An iterative distortion cancellation technique used in an orthogonal frequency division multiplexing system[15–17] is introduced to mitigate the nonlinear ISI. Furthermore, we have experimentally demonstrated a 40-Gbps 16-quadrature amplitude modulation (QAM) Mach-Zehnder modulator (MZM)-based VSB-IMDD half-cycle Nyquist-SCM system transmission over a 100-km uncompensated standard single-mode fiber (SSMF) with iterative nonlinear ISI cancellation. A cost-effective fiber Bragg grating (FBG) optical filter is used to realize the VSB filter. The experimental results show that 2.2-dB receiver sensitivity is improved at the forward error correction (FEC) limit. The iterative nonlinear ISI cancellation in a VSB-IMDD half-cycle Nyquist-SCM system can effectively suppress the destructive effect of the nonlinear ISI.

2 Theoretical Model

The principle of a VSB-IMDD half-cycle Nyquist-SCM system is shown in Fig. 1. The optical transmitter is a conventional half-cycle 16-QAM Nyquist-SCM modulation scheme.[1] A VSB filter is placed after the intensity modulator to achieve vestigial sideband transmission. At the receiver, O-FDE is carried out after downconversion to compensate the linear distortion based on the block-to-block operation.[8]

*Address all correspondence to: Na Liu, E-mail: liunana@bupt.edu.cn

0091-3286/2014/$25.00 © 2014 SPIE

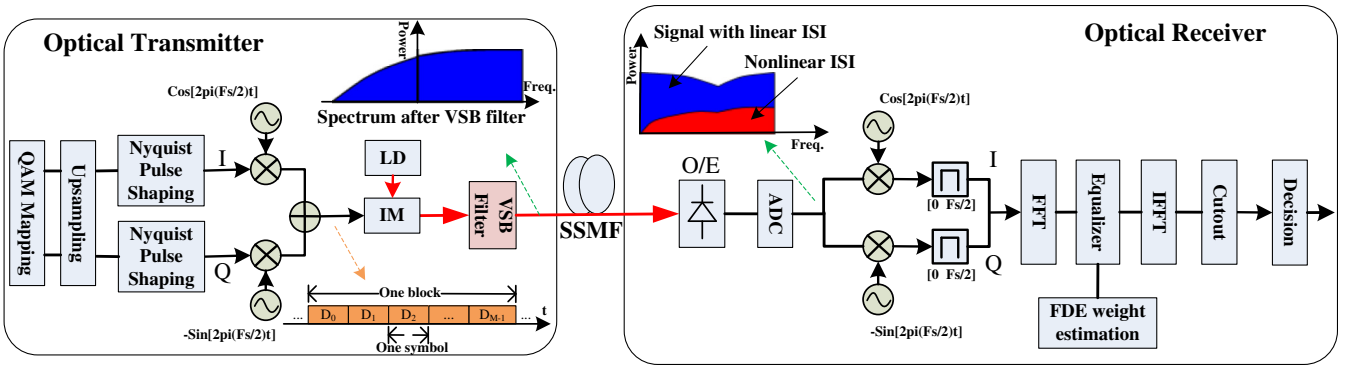

Fig. 1 Principle of vestigial sideband intensity modulation and direct detection (VSB-IMDD) half-cycle Nyquist–subcarrier modulation (SCM) system.

In this section, a theoretical model is built to analyze the causes of ISI in a VSB-IMDD single carrier system. In this model, M continuous symbols, $[D_0, D_1 \ldots D_{M-1}]$, combine as a block, as shown in Fig. 1. The block before the intensity modulator can be expanded into a Fourier series, $V = \Re\{\sum_{n=1}^{N} v_n e^{jn\omega t}\}$, where ω is the first-order harmonic, v_n is the complex information of the n'th-order harmonic, N is the index of the highest-order harmonic, and $\Re\{\cdot\}$ represents the real part. Assuming the intensity modulator is a linear electro-optic system with a constant chirp parameter α, the normalized optical power envelop can be written as $P = 1 + X_1$, where $X_1 = \Re\{X_n\}$, $X_n = r\sum_{n=1}^{N} v_n e^{jn\omega t}$. r is a scaling constant used to set an appropriate optical modulation index (OMI), where $\text{OMI} = r\sqrt{\sum_{n=1}^{N} |v_n|^2}$.[18] Accordingly, the normalized envelope of the optical field can be approximated as $E = 1 + \frac{1-j\alpha}{2} X_1 - \frac{1+\alpha^2}{8} X_2$, where X_2 is the second-order term, $X_2 = X_1^2 = \Re\{X_{2n}\}$, $X_{2n} = \sum_{n=1}^{2N} \tilde{x}_n e^{j(n\omega t + \tilde{\theta}_n)}$,[14] and the higher-order terms of v_n are disregarded. After the VSB filter, the first- and second-order terms can be expressed as

$$X_{1,\text{VSB}} = \frac{1}{2} r \sum_{n=1}^{N} H_{\text{USB}}(n) v_n e^{jn\omega t} + \frac{1}{2} r \sum_{n=1}^{N} H_{\text{LSB}}(n) v_n e^{-jn\omega t}$$

and

$$X_{2,\text{VSB}} = \frac{1}{2} \sum_{n=1}^{2N} H_{\text{USB}}(n) \tilde{x}_n e^{j(n\omega t + \tilde{\theta}_n)} + \frac{1}{2} \sum_{n=1}^{2N} H_{\text{LSB}}(n) \ \tilde{x}_n e^{-j(n\omega t + \tilde{\theta}_n)},$$

where H_{USB} and H_{LSB} are the frequency responses of the VSB filter in the upper sideband and lower sideband. Then the optical field can be expressed as

$$E_{\text{VSB}} = H(0) + \frac{\sqrt{1+\alpha^2}}{2} e^{-j\theta_\alpha} X_{1,\text{VSB}} - \frac{1+\alpha^2}{8} X_{2,\text{VSB}}, \quad (1)$$

where $\theta_\alpha = \tan^{-1}\alpha$, and $H(0)$ denotes the frequency response of the VSB filter at the optical carrier. After transmission with a distance L, the group-velocity dispersion parameter β_2, and no fiber loss, the response of the fiber transmission can be expressed as $H_{\text{CD}}(n) = e^{jn^2\theta_D}$, where $\theta_D = \beta_2 L\omega^2/2$. Thus, if $\Theta\{\cdot\}$ represents a signal after dispersive transmission, then

$$\Theta\{X_{1,\text{VSB}}\} = \frac{1}{2} r \sum_{n=1}^{N} H_{\text{USB}}(n) v_n e^{jn\omega t} e^{jn^2\theta_D} + \frac{1}{2} r \sum_{n=1}^{N} H_{\text{LSB}}(n) v_n e^{-jn\omega t} e^{jn^2\theta_D},$$

$$\Theta\{X_{2,\text{VSB}}\} = \frac{1}{2} \sum_{n=1}^{2N} H_{\text{USB}}(n) \tilde{x}_n e^{j(n\omega t + \tilde{\theta}_n)} e^{jn^2\theta_D} + \frac{1}{2} \sum_{n=1}^{2N} H_{\text{LSB}}(n) \tilde{x}_n e^{-j(n\omega t + \tilde{\theta}_n)} e^{jn^2\theta_D}.$$

Accordingly, the optical field becomes

$$E_{\text{CD}} = H(0) + \frac{\sqrt{1+\alpha^2}}{2} e^{-j\theta_\alpha} \Theta\{X_{1,\text{VSB}}\} - \frac{1+\alpha^2}{8} \Theta\{X_{2,\text{VSB}}\}. \quad (2)$$

The received signal after square-law photodetection is

$$R = |E_{\text{CD}}|^2 \cong [H(0)]^2 + \sqrt{1+\alpha^2} H(0) \Re[e^{-j\theta_\alpha} \Theta(X_{1,\text{VSB}})] + \frac{1+\alpha^2}{4} \{|\Theta(X_{1,\text{VSB}})|^2 - H(0) \Re[\Theta(X_{2,\text{VSB}})]\}. \quad (3)$$

The first term in Eq. (3) is the direct current component, the second term contains the desired block signal, and the third term represents the nonlinear distortion of block signal.

From Eq. (3), without the VSB filter, that is $H(0) = H_{\text{VSB}}^{\text{USB}}(n) = H_{\text{VSB}}^{\text{LSB}}(n) = 1$, the second term can be written as

$$\sqrt{1+\alpha^2} r \sum_{n=1}^{N} \cos(n^2\omega^2\beta_2 L/2 - \theta_\alpha) |v_n| \cos(n\omega t + \varphi_n),$$

where $|v_n|$ and φ_n are the amplitude and phase of the n'th-order harmonic, namely $v_n = |v_n| e^{j\varphi_n}$. The power of the desired block signal is proportional to $(1+\alpha^2)\cos^2(n^2\omega^2\beta_2 L/2 - \theta_\alpha)$, which is the equation for power

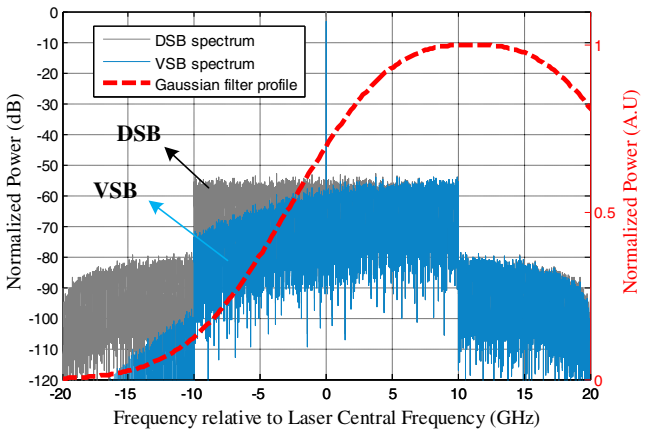

Fig. 2 Optical spectrum before and after VSB filter, and the Gaussian filter profile.

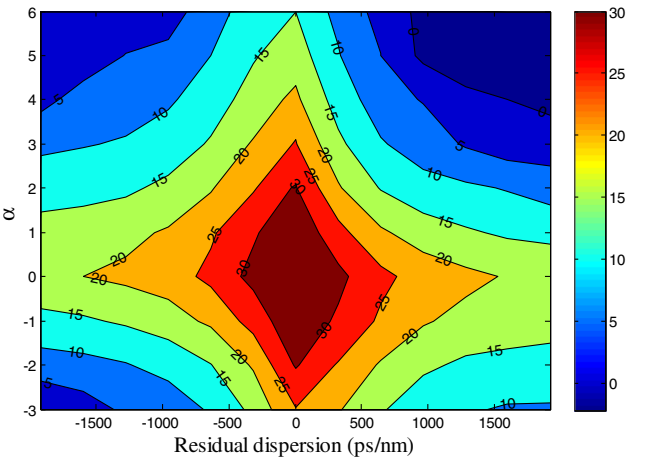

Fig. 4 Signal to nonlinear intersymbol interference (ISI) ratio (in decibels) versus dispersion and chirp.

fading.[14] If there is a VSB filter, then the second term can be written as

$$\frac{\sqrt{1+\alpha^2}}{2} rH(0) \sum_{n=1}^{N} \sqrt{a^2(n)+b^2(n)}|v_n|\cos(n\omega t+\varphi_n+\theta_n'),$$

where

$$a(n)+jb(n) = H_{\mathrm{USB}}(n)e^{j(n^2\theta_D-\theta_\alpha)} + H_{\mathrm{LSB}}(n)e^{-j(n^2\theta_D-\theta_\alpha)}$$

and θ_n' is the compound angle of $a(n)+jb(n)$. The block signal suffers from dispersion-, chirp- and VSB filter-related linear distortion. Figure 2 shows the normalized power spectrum before and after the VSB filter, where the VSB filter is a 1.35th-order Gaussian profile whose bandwidth and frequency offset are 21.7 and 11 GHz to match the FBG-based VSB filter employed in the following experiment. Figures 3(a) and 3(b) show the amplitude and phase transfer functions after 100-km SSMF transmission, which can be used as FDE weights to compensate the linear ISI. As shown in Fig. 3(a), the power null point could be erased after the VSB filter. But the amplitude difference between the maximum and the minimum is still 7 dB, which could be reduced by using a higher-order Gaussian filter. The phase transfer function is different from that of a single-sideband signal because the VSB signal contains a vestige of the suppressed sideband.

The effect of dispersion-, chirp-, and VSB filter-induced nonlinear ISI on the transmission performance is studied by numerical simulation. Without considering any noise, the signal to nonlinear ISI ratio (SIR), namely the ratio of the second term to the third term in Eq. (3), is used to measure the impact of nonlinear ISI on the system performance, where the linear ISI of the second term is fully compensated. In the simulation, we adopt a 16-QAM modulation format and zero roll-off raised-cosine pulse shaping. Then a 10-Gbaud (F_s) signal is upconverted on a 5-GHz ($F_s/2$) subcarrier. The VSB filter is the same as that in Fig. 2. The SIR as a function of dispersion and chirp is shown in Fig. 4. The results show that the SIR decreases after positive or negative dispersion transmission, and both positive and negative chirp further reduce the SIR. So the fiber dispersion and chirp of the modulator increase the nonlinear ISI and are detrimental to the VSB-IMDD system performance. The main reason for the finite SIR at back-to-back (B2B) is that the VSB optical filter destroys the linear relationship of the modulation voltage and the output optical power in the DD system. Thus, the nonlinear ISI is the bottleneck of the VSB-IMDD single carrier system. Therefore, in the following experiment, a chirp-free MZM is employed as an intensity modulator to reduce the nonlinear ISI and enhance the system performance.

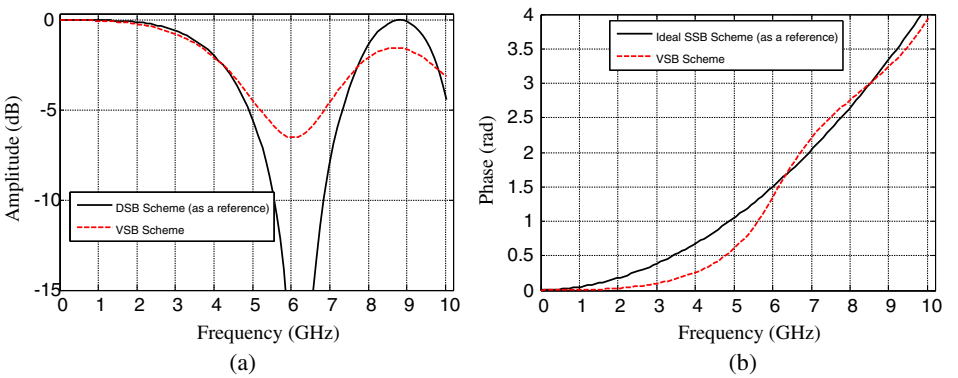

Fig. 3 (a) Amplitude and (b) phase transfer functions after 100-km standard single-mode fiber (SSMF) transmission (dispersion of 1600 ps/nm).

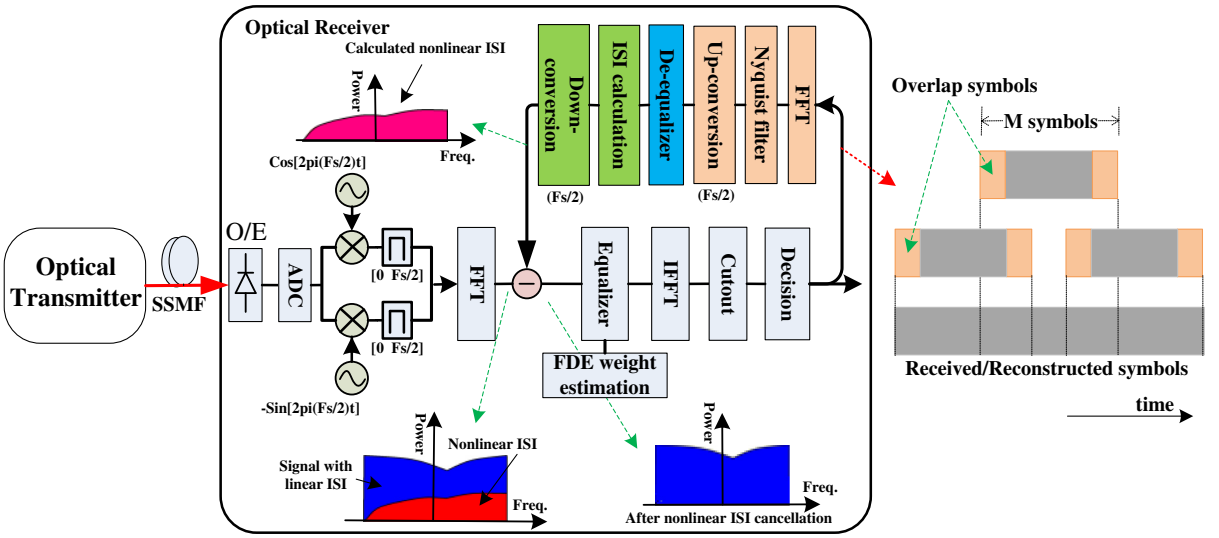

Fig. 5 Principle of ISI cancellation technique.

3 Principle of ISI Cancellation

To mitigate the influence of the nonlinear ISI, the iterative nonlinear ISI cancellation technique is introduced at the receiver, as shown in Fig. 5. The optical transmitter is the same as that in Fig. 1. At the receiver, after demodulating by the O-FDE method, the detected data are used to calculate the nonlinear ISI based on the theoretical model and the calculated results are further fed back to carry out the nonlinear ISI cancellation in the frequency domain with respect to each block. Then the received data after the nonlinear ISI cancellation are demodulated again to get the more correct detected data.

Based on the analysis in the second part, the nonlinear ISI could be estimated and eliminated by iteratively replacing $[D_0, D_1 \ldots D_{M-1}]^{(i)}$ by the detected data $[D_0, D_1 \ldots D_{M-1}]^{(i-1)}$, where the superscript, i, denotes the number of iterations. The nonlinear ISI cancellation is composed of three parts: a Nyquist intermediate frequency (IF) signal reconstruction, a channel de-equalization, and a nonlinear ISI calculation. In the block of the Nyquist IF signal reconstruction, as shown in Fig. 6, fast Fourier transform (FFT) is performed on the detected QAM data $[D_0, D_1 \ldots D_{M-1}]^{(i-1)}$ in a block. Then Nyquist pulse shaping and upconversion are completed in the frequency domain. The output of the n'th-order harmonic can be written as $v_n^{(i)}$. The first-order term, $X_1^{(i)}$, and the second-order term, $X_2^{(i)} = [X_1^{(i)}]^2$, of the block signal can be reconstructed. The OMI of transmitter is known in advance for the receiver, so the optical carrier value, A, can be reconstructed by $\mathrm{OMI} = \sqrt{(\sum_{n=1}^{N} |v_n^{(i)}|^2)/N}/A$. Then A, $X_1^{(i)}$, and $X_2^{(i)}$ are sent to the channel de-equalization block.

In the channel de-equalization block, the response of the VSB filter is known in advance, so the signal after the VSB filter can be calculated as $AH(0)$, $X_{1,\mathrm{VSB}}^{(i)}$, and $X_{2,\mathrm{VSB}}^{(i)}$. The fiber response can be estimated from the equalizer. Then the signal after fiber transmission, $\Theta\{X_{1,\mathrm{VSB}}^{(i)}\}$ and $\Theta\{X_{2,\mathrm{VSB}}^{(i)}\}$, can be achieved and sent to the block of the nonlinear ISI calculation.

From Eq. (3), the nonlinear ISI is composed of the beating and intermixing terms, which are, respectively, caused by the beating between the first-order terms, $\Theta\{X_{1,\mathrm{VSB}}^{(i)}\}$, and the mixing beating among the optical carrier, $AH(0)$, and the second-order term, $\Theta\{X_{2,\mathrm{VSB}}^{(i)}\}$. Consequently, following the process of nonlinear ISI calculation, the beating term, $\frac{1+\alpha^2}{4}|\Theta\{X_{1,\mathrm{VSB}}^{(i)}\}|^2$, and the intermixing terms, $-\frac{1+\alpha^2}{4}AH(0)\,\Re[\Theta(X_{2,\mathrm{VSB}}^{(i)})]$, of each harmonic could be individually calculated in the frequency domain. The nonlinear ISI is the sum of the two terms. After downconversion, the nonlinear ISI is fed back to be cancelled. The above process is applied

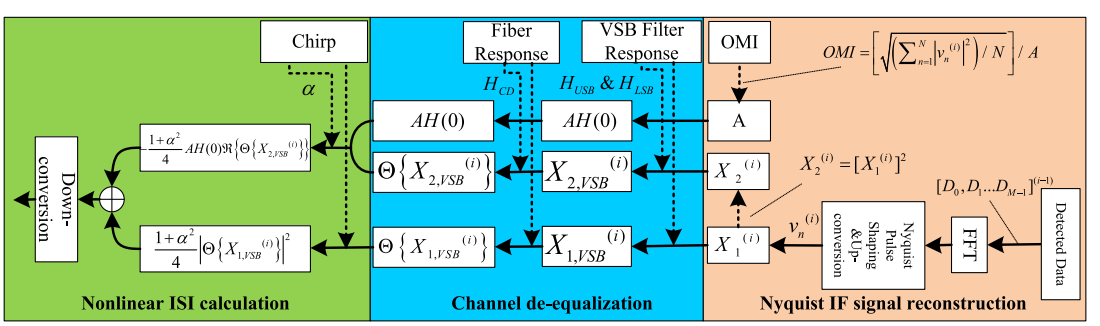

Fig. 6 The block diagram of nonlinear ISI calculation.

to all received signals with a sliding M-received-symbol in each block as shown in Fig. 5.

The computational complexity of the proposed nonlinear ISI cancellation technique mainly comes from inverse fast fourier transformation (IFFT), FFT, and the nonlinear ISI calculation as shown in Fig. 5. IFFT and FFT require $(2N) \times \log_2(2N)$ complex multiplications, and the nonlinear ISI calculation requires $(2N) \times \log_2(2N)$ complex multiplications.[15,19] Thus, the extra computational complexity of $(4N) \times \log_2(2N)$ is required for each iteration.

4 Experimental Setup and Results

To verify the efficiency of the nonlinear ISI cancellation, an equivalent experiment is performed and the experimental setup for the 40-Gbps FBG-based VSB-IMDD half-cycle Nyquist-SCM transmission system over 100-km SSMF is shown in Fig. 7. The electrical Nyquist baseband signal is generated by an Agilent® arbitrary waveform generator (AWG M8190A) using the MATLAB® program. Nevertheless, the sampling rate of the AWG is only 12 GSa/s, so we use an electro-optic-electro (E/O/E) conversion architecture to generate the 40-Gbps electrical Nyquist-SCM signal. Two sinusoidal signals divided from the same oscillator at 5 GHz are combined with the real and imaginary parts of the Nyquist baseband signals, respectively. Then the two combined signals are used to drive an in-phase/quadrature (IQ) modulator. The generated optical signal is a virtual single-sideband optical signal.[16] A 10-GBaud Nyquist-SCM signal will be obtained after photoelectric conversion. Since the Nyquist-SCM signal after O/E conversion suffers from distortions caused by hardware imperfections and signal-to-signal beating interference, two methods are adopted to mitigate the distortions and interference. First, the carrier-to-signal-power ratio (CSPR) is increased, which is the power ratio of the radio frequency tone to the Nyquist baseband signal. Second, the baseband signal after QAM mapping is predistorted. The ideal signal after QAM mapping can be written as $\vec{V} = [V_1, V_2 \ldots V_L]^T$, where L is the total number of symbols. The received signal after E/O/E conversion can be written as $\vec{R} = [R_1, R_2 \ldots R_L]^T$, which can be further expressed as $\vec{R} = \Gamma\{\vec{V}\}$, where $\Gamma\{.\}$ is the channel transfer function of the E/O/E conversion process. Assuming the received signal after E/O/E is the desired ideal signal, the transmitted signal should be predistorted, $\vec{V} = \Gamma\{\vec{Y}\}$, where $\vec{Y} = [Y_1, Y_2 \ldots Y_L]^T$ are the predistortion values. Iteration is used to increase the signal quality, $\vec{Y}^{(i)} = \vec{Y}^{(i-1)} + \eta\{\vec{V} - \Gamma[\vec{Y}^{(i-1)}]\}$, where the superscript, i, denotes the number of iterations, initial values, $\vec{Y}^{(0)} = \vec{V}$, and η is the scaling parameter. A smaller CSPR leads to instability of the iteration, while a larger CSPR reduces the photoelectric conversion efficiency.[16] Then the optimal CSPR, the iteration number, and η are set to be 15 dB, 2, and 1.

Based on the E/O/E architecture, the signal processing program at the transmitter consists of bit (a pseudorandom binary sequence with pattern length $2^{15} - 1$) to symbol mapping, predistortion, two times upsampling, Nyquist pulse shaping, and pre-emphasis. It is emphasized that the zero roll-off raised-cosine pulse shaping and pre-emphasis of the four level in-phase (I) and quadrature (Q) signals are realized using FDE (Ref. 20) for all symbols. The sample rate of 12 GSa/s is used to synthesize the 5-GHz baseband signal. After E/O/E conversion, a 10-GBaud Nyquist-SCM signal is obtained and used to drive an MZM to generate an optical DSB signal. The electrical spectra after AWG, before the IQ modulator, after PD, and before MZM are shown in Figs. 7(i)–7(iv). A commercial FBG is used as a VSB filter with temperature compensation and a profile of a 1.35th-

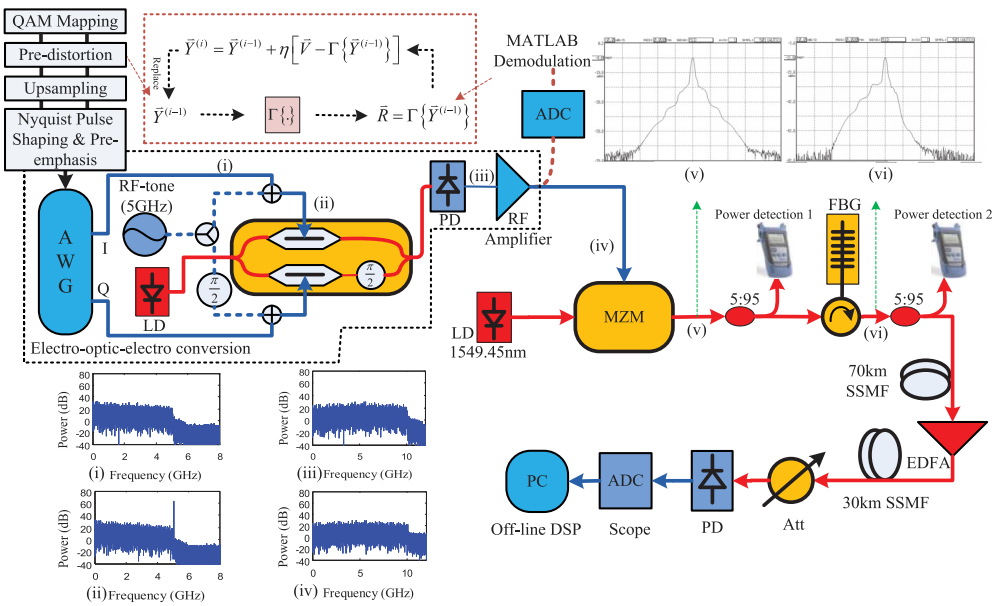

Fig. 7 Experimental setup of fiber Bragg grating (FBG)-based VSB-IMDD half-cycle Nyquist-SCM transmission system. The electrical spectra (i) after arbitrary waveform generator, (ii) before in-phase/quadrature modulator, (iii) after PD, and (iv) before Mach-Zehnder modulator. The optical spectra (v) before and (vi) after FBG filter.

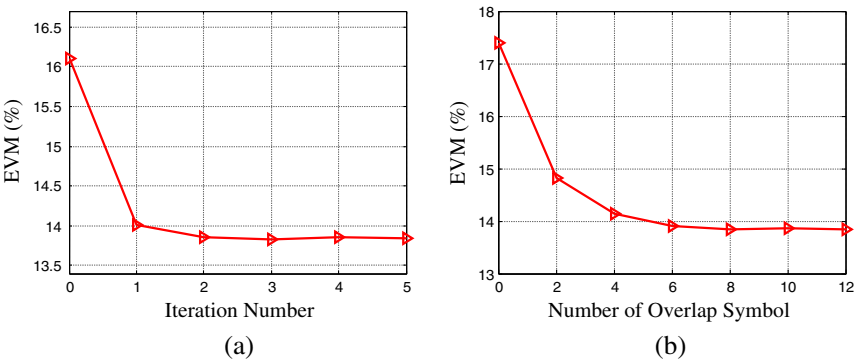

Fig. 8 Measured error vector magnitude versus (a) the iteration number and (b) the number of overlap symbola after 100-km SSMF transmission with a received power of −3 dBm.

order Gaussian, whose 3-dB bandwidth is 21.7 GHz. The optical power difference before and after the VSB filter is used as a feedback to precisely adjust the central frequency of the laser; then the central frequency offset of the VSB filter relative to the optical carrier can be stabilized at 11 GHz. The insertion loss of the FBG filter is ∼3.5 dB. The optical spectra before and after the FBG filter are shown in Figs. 7(v) and 7(vi), which are measured by a conventional optical spectrum analyzer with a 0.02 nm resolution. The launch power is 4 dBm, and an erbium doped fiber amplifier with a 16-dB gain is inserted after the 70-km SSMF transmission. After a 100-km transmission, a power attenuator is used to adjust the received power. The received electrical signal is captured by a LeCroy® digital oscilloscope WaveMaster813ZI-A with a 40-GSa/s sampling rate and is processed off-line by MATLAB® DSP program. The received signal is downsampled to 20 GSa/s (two samples per symbol) and then downconverted to produce separate I and Q signals. The linear ISI of the second term in Eq. (3) is compensated by the O-FDE method with an FFT size of 1024 ($M = 512$ symbols) and enough overlapping symbols, followed by the symbol to bit mapping, error vector magnitude (EVM) calculation, and bit error counting. The detected data are used to reconstruct the raw signals and calculate the nonlinear ISI. The Nyquist pulse shaping and upconversion in the iteration loop is two times oversampling (equivalently 20 GSa/s). The nonlinear ISI of each harmonic is individually calculated in the frequency domain and then cancelled.

Figure 8(a) shows the EVM versus the iteration number after a 100-km SSMF transmission with a received power of −3 dBm and overlap symbols of 20. The iterative process would yield more accurate estimated nonlinear ISI values and more correct detected data. The EVM performance is no longer improved after the second iteration. However, the computation complexity of iteration increases linearly. So the iteration number is set to be two in the following experiment.

The measured EVM versus the number of overlap symbols on one side of a block after a 100-km SSMF transmission with an iteration number of two is shown in Fig. 8(b). Nyquist pulse shaping makes the signal bandwidth become narrow and the pulse trailing will spread into adjacent time slots. But the reconstructed Nyquist pulses through the FDE suffer from distortions at the beginning and the end in one block. So the truncated pulses affect the accuracy of the nonlinear distortion calculation in the iterative loop. Therefore, the symbol number of overlap region covers not only the pulse extension induced by dispersion, but also the pulse

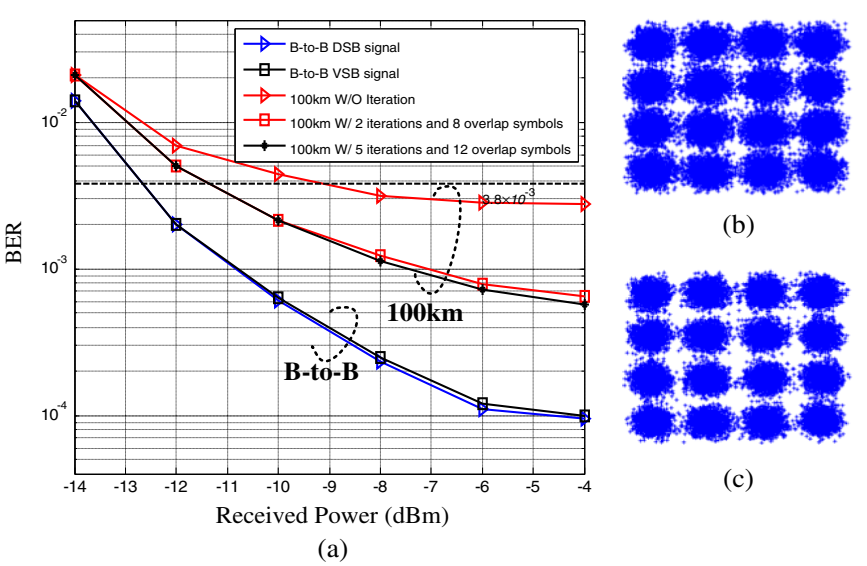

Fig. 9 (a) Measured BER versus the received power. The constellations (b) before and (c) after nonlinear ISI cancellation.

trailing. The EVM converges to 13.8% when the number of overlap symbols is greater than or equal to eight. So the number of overlap symbols is fixed to be eight.

The measured BER as a function of the received power with and without nonlinear ISI cancellation and the corresponding constellations are shown in Figs. 9(a)–9(c). The DSB signal and the VSB signal at B2B exhibit a BER floor of 0.91×10^{-4} (EVM 11.09%) and 0.98×10^{-4} (EVM 11.15%), respectively. Compared with two iterations and eight overlap symbols, the system performance with five iterations and 12 overlap symbols is not significantly increased. The BER of 3.8×10^{-3} (the FEC limit[21]) can be obtained at the received powers of −9.2 and −11.4 dBm. Accordingly, the 2.2-dB receiver sensitivity is improved after using the nonlinear ISI cancellation technique. Moreover, compared with the B2B case, only a 1.4-dB penalty is shown after a 100-km SSMF transmission.

5 Conclusion

In this paper, the dispersion-, chirp-, VSB-, and square-law detection-induced linear and nonlinear ISI in a single carrier system are analyzed theoretically and numerically. Based on the theoretical analysis, we propose and experimentally demonstrate an iterative nonlinear ISI cancellation technique in a 40-Gbps 16-QAM MZM-based VSB-IMDD half-cycle Nyquist-SCM system over a 100-km uncompensated SSMF transmission. The 2.2-dB receiver sensitivity improvement can be achieved at the FEC limit by using the iterative nonlinear ISI cancellation.

Acknowledgments

This study is supported by National High Technology Research and Development Program of China (No. 2012AA011303) and Fund of State Key Laboratory of Information Photonics and Optical Communications (Beijing University of Posts and Telecommunications), China.

References

1. A. S. Karar and J. C. Cartledge, "Generation and detection of a 112-Gb/s dual polarization signal using a directly modulated laser and half-cycle 16-QAM Nyquist-subcarrier-modulation," presented at *European Conf. and Exhibition on Optical Communication*, Amsterdam, Netherlands, Th.3.A.4 (2012).
2. J. C. Cartledge and A. S. Karar, "100 Gbit/s using intensity modulation and direct detection," in *European Conf. and Exhibition on Optical Communication*, London, pp. 618–620 (2013).
3. Y. Kim et al., "Optimization of transmission performance of 10-Gb/s optical vestigial sideband signals using electrical dispersion compensation by numerical simulation," *IEEE J. Sel. Topics Quantum Electron.* **10**(2), 371–375 (2004).
4. J. Lee et al., "Optically preamplified receiver performance due to VSB filtering for 40-Gb/s optical signals modulated with various formats," *J. Lightwave Technol.* **21**(2), 521–527 (2003).
5. X. Wei and J. Leuthold, "Relation between vestigial-sideband filtering and pi/2 progressive phase shift," *Opt. Lett.* **29**(14), 1599–1601 (2004).
6. W. Idler et al., "Vestigial side band demultiplexing for ultra high capacity (0.64 bit/s/Hz) transmission of 128×40 Gb/s channels," in *Optical Fiber Communication Conf./National Fiber Optic Engineers Conf.*, Anaheim, California, p. MM3-1 (2001).
7. P. M. Watts et al., "Performance of single-mode fiber links using electronic feed-forward and decision feedback equalizers," *IEEE Photon. Technol. Lett.* **17**(10), 2206–2208 (2005).
8. K. Ishihara et al., "Frequency-domain equalisation without guard interval for optical transmission systems," *Electron. Lett.* **44**(25), 1480–1482 (2008).
9. K. Ishihara et al., "Frequency-domain equalization for coherent optical transmission systems," in *Optical Fiber Communication Conf./National Fiber Optic Engineers Conf.*, Los Angeles, California, pp. 1–3 (2011).
10. J. Prat et al., "Square root strategy: a novel method to linearize an optical communication system with electronic equalizers," in *European Conf. and Exhibition on Optical Communication*, Glasgow, Scotland, Vol. 3, pp. 713–714 (2005).
11. C. Xia and W. Rosenkranz, "Nonlinear electrical equalization for different modulation formats with optical filtering," *J. Lightwave Technol.* **25**(4), 996–1001 (2007).
12. S. Färbert et al., "Performance of a 10.7 Gb/s receiver with digital equaliser using maximum likelihood sequence estimation," presented at *European Conf. and Exhibition on Optical Communication*, Stockholm, Sweden, Th.4.1.5 (2004).
13. S. Napoli et al., "Limits of maximum-likelihood sequence estimation in chromatic dispersion limited systems," presented at *Optical Fiber Communication Conf./National Fiber Optic Engineers Conf.*, Anaheim, California, JThB36 (2006).
14. C.-C. Wei, "Small-signal analysis of OOFDM signal transmission with directly modulated laser and direct detection," *Opt. Lett.* **36**(2), 151–153 (2011).
15. D.-Z. Hsu et al., "SSII cancellation in an EAM-based OFDM-IMDD transmission system employing a novel dynamic chirp model," *Opt. Express* **21**(1), 533–543 (2013).
16. W.-R. Peng et al., "Spectrally efficient direct-detected OFDM transmission incorporating a tunable frequency gap and an iterative detection techniques," *J. Lightwave Technol.* **27**(24), 5723–5735 (2009).
17. C. Ju, X. Chen, and Z. Zhang, "40 Gbps 100-km SSMF VSB-IMDD OFDM transmission experiment based on SSII cancellation and FBG-filtering," presented at *Optical Fiber Commun. Conf./National Fiber Optic Engineers Conf.*, San Francisco, California, Tu2G.6 (2014).
18. G. P. Agrawal, *Fiber-Optic Communication Systems*, 3rd ed., John Wiley, New York (2002).
19. C.-C. Wei, "Analysis and iterative equalization of transient and adiabatic chirp effects in DML-based OFDM transmission systems," *Opt. Express* **20**(23), 25774–25789 (2012).
20. J. Wang, C. Xie, and Z. Pan, "Generation of spectrally efficient Nyquist-WDM QPSK signals using digital FIR or FDE filters at transmitters," *J. Lightwave Technol.* **30**(23), 3679–3686 (2012).
21. ITU-T Recommendation G.975.1, "Forward error correction for high bit-rate DWDM submarine systems," Appendix I.9 (2004).

Na Liu received her bachelor's degree from Xi'an University of Posts and Telecommunications, China, in 2010. She is currently working toward her PhD degree in the State Key Lab of Information Photonics and Optical Communications, Beijing University of Posts and Telecommunications. Her current research interest is impairment compensation in intensity modulation and direction detection systems.

Biographies of the other authors are not available.